Taylor & Francis
Taylor & Francis Group

RESEARCH ARTICLE

Development of a thermal excitation source used in an active thermographic UAV platform

Shakeb Deane [a], Nicolas P. Avdelidis[a,b], Clemente Ibarra-Castanedo[b], Alex A. Williamson[c], Stephen Withers[d], Argyrios Zolotas[a], Xavier P. V. Maldague [b], Mohammad Ahmadi[b], Shashank Pant[e], Marc Genest[e], Hobivola A. Rabearivelo[f] and Antonios Tsourdos[a]

[a]Cranfield University, School of Aerospace, Transport and Manufacturing, Cranfield MK43 0AL, United Kingdom; [b]Laval University, Department of Electrical and Computer Engineering, Computer Vision and Systems Laboratory, Quebec City, QC, G1V 0A6, Canada; [c]Mapair Thermography Ltd, Melbourn, Royston SG8 6HD, United Kingdom; [d]Innovative Technology & Science Ltd, North Wing, Old Livery, Hildersham Road, Cambridge, CB21 6DR, United Kingdom; [e]National Research Council Canada, Ottawa, ON, K1A 0R6, Canada; [f]BI Expertise, 830 Ernest-Gagnon Suite 315, Quebec City, QC, G1S 3R3, Canada

ABSTRACT

This work aims to address the effectiveness and challenges of using active infrared thermography (IRT) onboard an unmanned aerial vehicle (UAV) platform. The work seeks to assess the performance of small low-powered forms of excitation which are suitable for active thermography and the ability to locate subsurface defects on composites. An excitation source in multiple 250 W lamps is mounted onto a UAV and is solely battery powered with a remote trigger to power cycle them. Multiple experiments address the interference from the UAV whilst performing an active IRT inspection. The optimal distances and time required for a UAV inspection using IRT are calculated. Multiple signal processing techniques are used to analyse the composites which help locate the sub-surface defects. It was observed that a UAV can successfully carry the required sensors and equipment for an Active thermographic NDT inspection which can provide access to difficult areas. Most active thermographic inspection equipment is large, heavy, and expensive. Furthermore, using such equipment for the inspection of complex structures is time-consuming. For example, a cherry picker would be required to inspect the tail of an aircraft. This solution looks to assist engineers in inspecting complex composite structures and could potentially significantly reduce the time and cost of a routine inspection.

1. Introduction

The use of unmanned aerial vehicles (UAVs) for the remote inspection of large and/or inaccessible areas has increased in popularity in recent times due to their versatility and inclusion of onboard measuring instruments. The advancement in technology has contributed to making UAVs more affordable, accessible, and safer to deploy. Technological

developments have also had a great impact on a variety of sensors, which are now smaller, lighter, and with improved performance. The sensors enable a UAV to be used for remote non-destructive testing (NDT) inspections and many other applications.

NDT is a method used to evaluate materials within a structure. Composite usage in aircraft has increased massively due to their excellent strength-to-weight ratio. Aircraft today have increased fuel efficiency due to the reduced weight of the structure. However, when composites are subject to damage, the material reacts differently than traditional homogeneous materials would. For example, the result of impact damage on an aluminium aircraft skin would commonly result in a visible dent whereas, impact damage on composite materials would result in damage such as delamination or cracks that are barely visible to the human eye. Furthermore, given the layered nature of some composites and the (variable) orientation of the fibre filaments, damage often propagates deeper and wider than the surface indication may suggest.

Several methods of inspecting composite materials can be used to locate such damage. Some inspection methods come with limitations such as expensive equipment, contact-based inspection, or destructive testing. Infrared Thermography (IRT) is used to capture thermal patterns across a area of interest. UAVs being used for IRT are ideal for a contactless survey of large and complex composite structures.

There has been not much development for UAV active thermography due to several limiting factors. Active Thermography is a method that is ideal for a lab environment where there are minimum hardware limitations and external parameters. With the advancement in IR camera technology, an uncooled IR camera can achieve an acceptable NDT standard. Due to most uncooled cameras being small, lightweight, and affordable, they are more accessible to use on a UAV. Nevertheless, an adequate excitation source for the UAV needs to be developed. The excitation source needs to be small and able to produce enough thermal stimulation to induce a contrast difference in the thermal images where a defect is present.

The following research explores the possibility of mounting an effective IR excitation source on a UAV platform. A UAV with an onboard IR camera and excitation source will allow the platform to perform static (hovering) or dynamic (scanning) inspections using IR

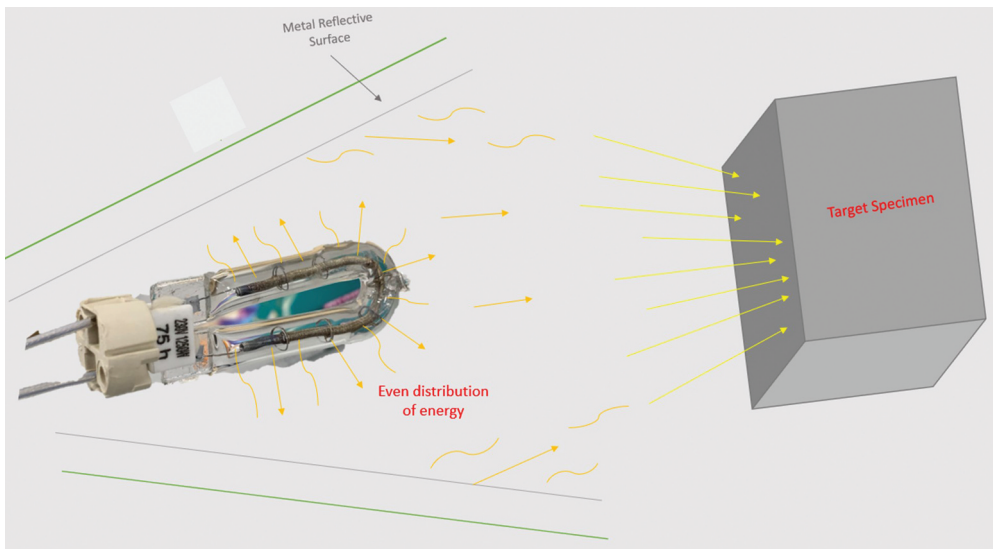**Figure 1.** UAV with active thermography capabilities.

Figure 2. Diagram showing the IR waves and light travelling from the bulb to the area of interest.

thermography. This will enable the inspection of large and complex structures with the ability to locate subsurface defects on composites. Figure 1 represents a UAV with active thermographic capabilities.

1.1. UAV Thermography

Thermography consists of analysing heat transfer from the surface of an object. Heat transfer is a complex and transient phenomenon that depends on a combination of factors. Thermal NDT can provide quantitative information about hidden defects or features in a material. The factors that need to be considered when performing such inspections are the thermal properties (e.g. conductivity, diffusivity, effusivity, specific heat), spectral properties (e.g. emissivity, absorption, reflection, transmission), and other physical characteristics such as density and porosity [1].

In the case of UAV-IRT, in addition to the above-mentioned factors, other aspects may have a significant impact on heat transfer and thermal data acquisition such as UAV movement instability and convection cooling from the propellers. This work will address the further challenges that UAV thermal NDT presents.

Table 1. Excitation source-250 W halogen bulb specs.

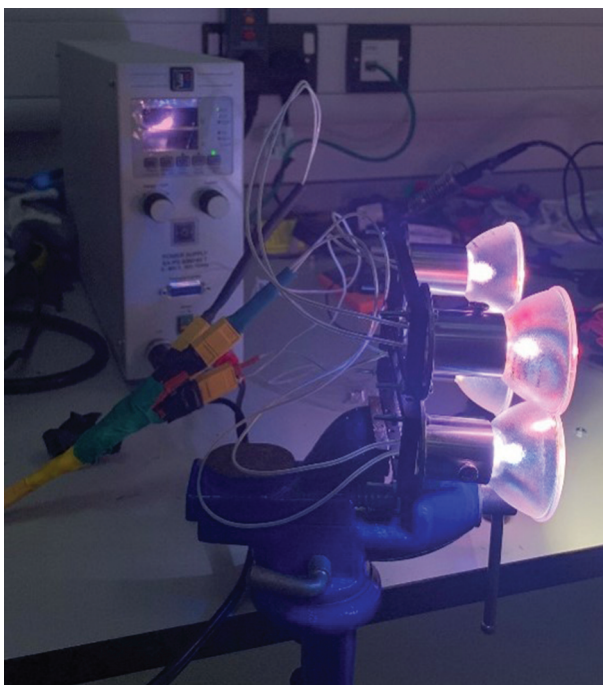|	
Colour Temp	3250 K
Focal Length	35 mm
Lumens	1200 lm
Diameter	51.0 mm
Length	44.8 mm
Life span	300 h
Weight	36 g
Coating	Dichroic

Figure 3. View of the halogen lamp array composed of four 250 W bulbs.

1.1.1. Passive IRT

The passive approach is commonly used in the investigation of materials that are naturally at different temperatures (usually higher than ambient). The presence of anomalies could be missed if the inspection is not performed at the 'correct' time. Building inspection (either UAV-based or other) is a good example of this as the outside environmental conditions affect the building temperature. Given the differences in thermo-physical properties among some materials react faster than others to these fluctuations. At a given moment, it is possible that two dissimilar materials attain approximately the same temperature and would not produce enough thermal contrast to be detectable by IRT. For some specific types of defects (humidity for instance), inspections can be conducted at moments when maximum thermal contrast is expected, such as early morning right after sunrise or late in the afternoon right after sunset, at these moments good conductors will heat up faster than insulators after exposed to solar irradiation and cool down faster after sunset [2].

Water ingress detection in honeycomb aircraft after a flight cycle can be common [3]. Within the honeycomb cells, water would be present as it would take longer to unfreeze after landing, compared to aluminium or composites. To detect, the thermogram will show cold spots. In summary, it is often possible to prepare a passive thermography inspection strategy to maximise the chances to identify anomalies. On a jet engine nacelle, there is a heat shield on one side and a perforated CFRP facesheet on the other side, this would be difficult to inspect using passive thermography [4]. However, Kidangan et. al. [4] proposes active thermography techniques such as flash thermography to access the inner layer.

Table 2. Wire size amp tolerances [7].

Size AWG	Insulation temp 60℃	Insulation temp 75℃	Insulation temp 90℃
12	20 A	25 A	30 A
10	30 A	35 A	40 A
8	40 A	50 A	55 A
6	55 A	65 A	75 A

1.1.2. Active IRT

Anomalies, cracks, and defects within aircraft structures are difficult to detect visually. Delamination, water ingress and other anomalies can be present sub-surface. Active thermography approach is preferred over passive because these features are difficult to see without thermal stimulation to induce a contrast difference within the thermal data. Active IR is effective as the thermal stimulation is with a controlled energy source, the captured data can be post-processed to improve detection and defect identification [5].

1.1.3. UAV-IRT

The major problems/limitations to take into consideration in UAV-IRT is that the drone must carry an excitation source along with the IR camera, RGB camera, and other fundamental sensors. The heating source, however, consumes considerable amounts of energy and would be difficult to operate for long periods on a battery-powered UAV. A Tethered cable would eliminate the power limitations, in doing so it would restrict the versatility of the UAV platform, although still practical for some specific applications such as the inspection of aircraft inside a hangar.
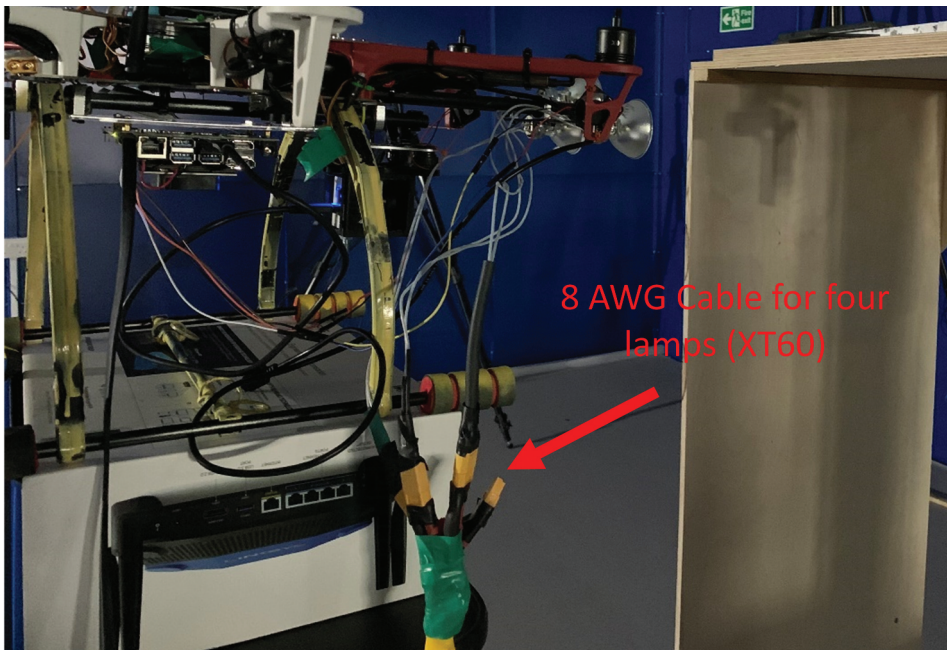

Figure 4. View of the lamp assembly connected using a 4-way split cable.

Table 3. A table displaying the temperature measurement probe, the number of bulbs, the voltage and any other information about the specific test.

Test #	# of bulbs	Probe location	Information	Voltage (V)
TEST 1	2	Bulb housing	Probe touching bulb housing	24
TEST 2	1	Sample	One metre -> sample	24
TEST 3	2	Sample	One metre -> sample	24
TEST 4	2	Sample	Half a metre -> sample	24
TEST 5	4	In-between lamps	No contact with lamp surface	24
TEST 6	4	Sample	Light -> Sample (half a metre distance)	24
TEST 7	4	Sample	Light -> Sample (one metre distance)	24
TEST 8	2	UAV cooling	10 Inch propellors	24
TEST 9	2	Sample	One metre distance with propellors on	24
TEST 10	2	Sample	Half a metre distance with propellors on	

Table 4. A table displaying the amps, and the different temperature measurements from the tests.

Test #	Amps (A)	Ambient temp °C	Temp °C after the 30s
TEST 1	21	20	130
TEST 2	10	20	21.1
TEST 3	21	20	22.5
TEST 4	21	20.9	26.4
TEST 5	42	20.03	70.2
TEST 6	42	21	29.4
TEST 7	43	21	23.5
TEST 8	21	21.7	39.2
TEST 9	21	21	22.7
TEST 10	21	21	24.7

There are multiple thermography inspection approaches that have different limitations. Thermography static acquisition requires several tests to cover the whole inspected area. This method is not suitable for UAV inspection due as it would not be time-efficient.

Line scan thermography is a dynamic inspection process that is much faster than the static pulsed technique since it can potentially scan large areas dynamically. It is however limited to the reach of the robot arm and the scanning speed, i.e. the faster the scanning speed the less deep the heat front can reach. A dynamic inspection will require data stabilisation and data reconstruction from dynamic to pseudo-static.

Pulsed thermography inspection will require the UAV to hover while capturing active thermographic data. The method is more complicated than static thermography due to flight instability, therefore the data captured will need to be stabilised. This approach will be used to inspect composites with the active thermographic UAV. The approach will likely speed up the capture time, but the post-processing will likely be challenging due to the video stabilisation and the pseudo-static data reconstruction.

In this work, an excitation source is developed for a UAV platform for the use of active thermography. The development would accelerate the dynamic UAV active infrared thermography system for the indoor inspection of large composite aircraft.

2. Experimental procedure I

2.1. UAV excitation source development

There are many things to consider when integrating a form of thermal excitation into a UAV. To predict the UAV flight time, it is necessary to calculate the mass and consumption of power. A small excitation source is essential for UAV integration, therefore the thermal transfer from the source to the target needs to be effective and the challenges to mount the source on the platform will be addressed.

Figure 2 shows a representation of the IR waves travelling from the lamp to the area of interest.

The energy reaching the target will be reduced if the distance of the excitation source increases from the target. Consequently, this will also increase the beam size. The inverse square law will allow us to calculate the amount of energy reaching the target area.

The purpose of the experiment is to focus on the infrared radiation emitted and not the visible light (lumens). Emitted radiation from the halogen lamp can be characterised by the relationship in Equation 1, regardless of the unit of radiation, all measures of exposure will drop off by the inverse square law. For example, if the distance is increased by a factor of two, the energy is spread over four times the area, meaning the beam will enlarge and the temperature will reduce as the energy has dissipated over an area four times that of the area from one metre away [6].

Equation 1: Radiation Inverse Square Law.

$$\frac{S}{4\pi r^2} = I \tag{1}$$

Description of variables:

- **S** = Source strength (w)
- **4πr^2** = Sphere area m^2
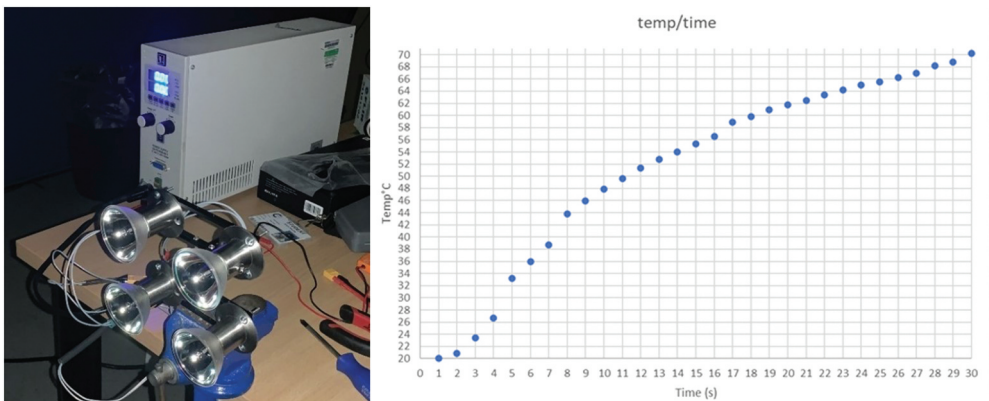- **I** = Intensity at the surface of a sphere (w/m^2)

Figure 5. (A) View of the experimental setup. The yellow arrow shows the probe position that is between all four lamps measuring the surrounding heat build up. **(B)** A temperature rise in between lamps over time.
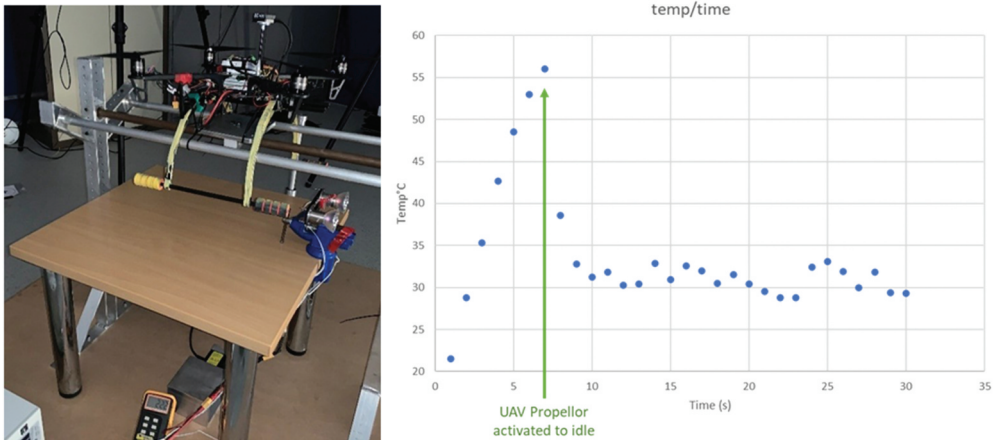
Figure 6. (A) Experimental setup of test 8. The yellow arrow points to the probe position. **(B)** Temperature rise of 250 w lamp surface over time before and after the effect of the UAV propellors.

From preliminary tests, it was concluded that a 1000 W halogen lamp would be an effective excitation source in terms of delivered energy to the inspected surface. However, this is the smallest lamp that could be found off the shelf, and it is over the preferred weight for the UAV. Attaching this lamp to the UAV will inevitably add more weight with the cables, batteries, and other necessary components required. For the final prototype, a 1000 W bulb will be used. The bulb needs to lose mass and the area of the excitation needs to be larger and uniform. One possible solution would be to use multiple bulbs at a smaller wattage equalling 1000 W.

2.1.1. UAV excitation source prototype

To comply with the weight and power limitations for the proposed UAV-IRT solution, a bespoke halogen lamps assembly has been chosen to integrate with the UAV. The specs of the bulbs can be seen in Table 1 and Figure 3 is an image of the lamp arrangement.

The lamp assembly can be powered with a direct current which eliminates the need for a powered tethered cable. A 6S battery will be used instead. The DC lamp allows for the capability of the excitation source to be powered onboard the UAV. The redesign will require multiple 250 W lamps onboard to ensure the target requires the most effective amount of infrared radiation, this will allow a successful active thermography test. The lamps are small enough to incorporate onto a UAV. The lamps will be mounted onto some carbon fibre poles due to their strength and weight efficiency. Carbon fibre will provide a stable mounting point and can withstand the heat generated from the lamps.

The lamps consume a significant amount of energy when powered, with a current of 10–11 amps each. A limitation of such a powerful excitation source is that it requires a thick and heavier cable. When powering four lamps from a single power source, the cable needs to be able to carry around 33 amps for three bulbs. Table 2 displays the number of amps that the different wire sizes can tolerate.

To power the bulbs in the lab for preliminary trials, an 8 AWG cable was used. The cable has four XT60 connectors, allowing the cable to power up to four lamps. Figure 4 shows the cable connected to the lamps.

Figure 7. View of the experimental setup of test 6 described in Table 3. The thermocouple probe is bonded to the sample using insulation tape on the cable, the probe is fully exposed.
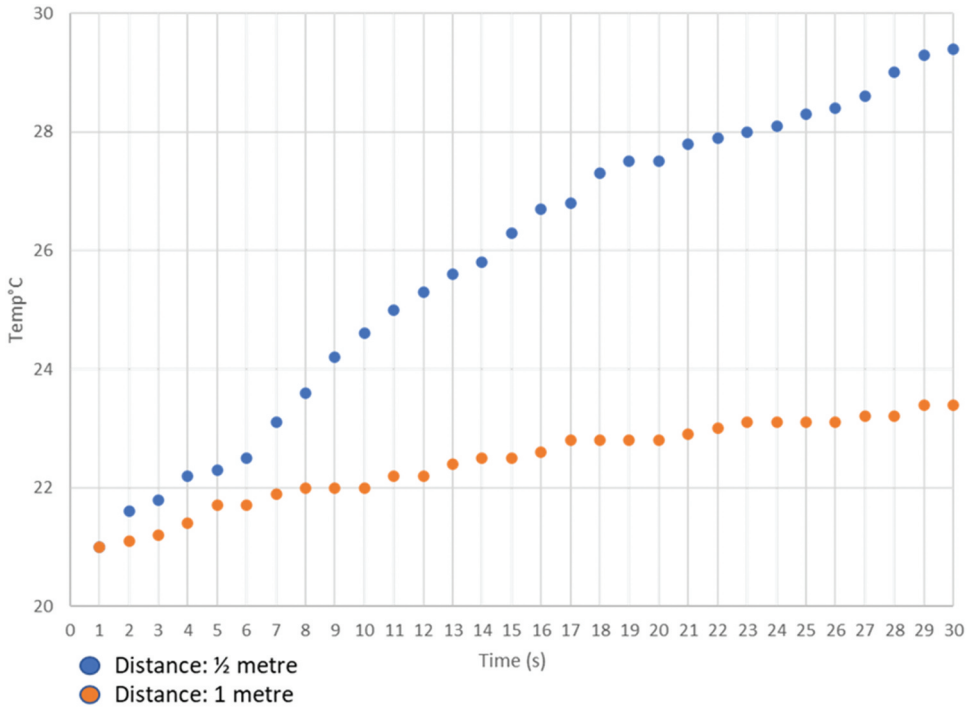

Figure 8. Surface temperature increase over time when heating a composite with the lamp assembly at both half a metre (blue dots) and one metre (Orange dots) from the sample.
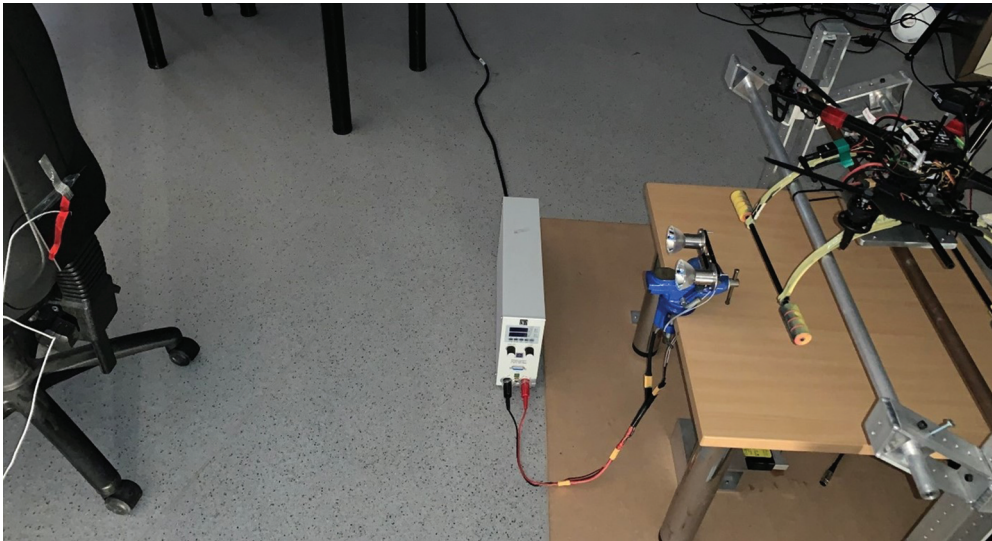
Figure 9. View of the experimental setup of tests 9 and 10.

A series of experiments were necessary to review the capabilities of the chosen lamps. The experiments were intended to achieve the following:

- Calculate the excitation source field of view from specific distances.
- Calculate the heating efficiency of composite samples from; half a metre and one-metre distances.
- Investigate the effect of UAV propellors on the bulb temperature and the sample heating.
- Demonstrate the feasibility of a multiple bulb arrangement onboard a UAV.

The purpose of the following test will determine the competency of the 250 W halogen bulbs for active thermography UAV inspections. Table 3 shows details of the ten experiments carried out and Table 4 shows the temperatures from the experiments.

2.1.1.1. Temperature measurement of the halogen lamps. Active thermography needs intense energy to excite the material to induce a contrast difference in the thermal camera captured data for defect identification. One of the 250 W halogen bulbs operated at full power will quickly reach extremely high temperatures, this could be a cause for concern as it is possible it could affect the surrounding components on the UAV. The aim is to understand the amount of heat that is emitted to ensure it is safe to mount on the UAV. A probe is measuring the temperature between four 250 W lamps. Figure 5A is an image of the experimental setup. In Figure 5B the graph shows the temperature over time. The temperature rapidly rises from ambient (20°C) to around 70°C in 30 seconds. From this experiment, it was established that a 30s heating threshold for the lamp assembly to be powered at once.
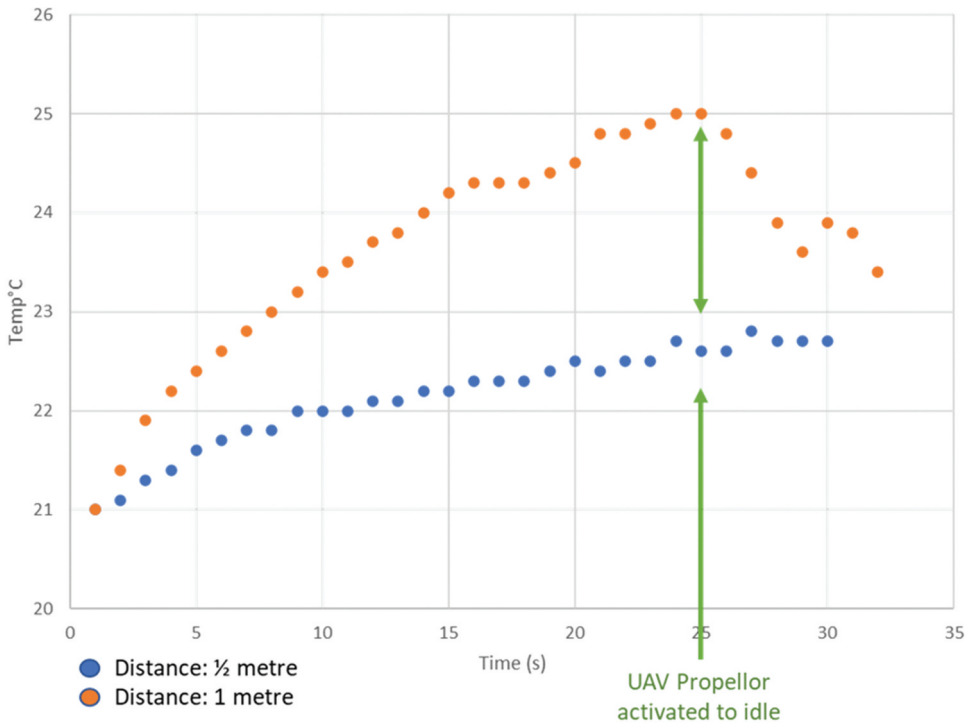
Figure 10. Temperature of the composite sample during excitation from the halogen lamps over 70 seconds, with the UAV propellers rotating. The blue dots represent the sample half a metre away from the UAV and lamps and the Orange dots represent the sample one metre away from the UAV and lamps.

2.1.1.2. Propellor cooling effect on the bulbs. In this test, a probe will measure the surface temperature of the dichroic coated reflectors over time during the power cycle. In the previous test, the lamp surface temperature reached 130°C after 30 seconds (Table 4). The following experiment was intended to investigate the cooling effect of the propellors on the bulbs. The experimental setup is shown in Figure 6A, the UAV is constrained to a rig while the bulbs are held on a vice directly below. The probe is located on the lamp surface. The lamps were switched on, and the temperature kept rising exponentially. In Figure 6B at seven seconds the temperature drops rapidly, as this was when the UAV was powered up and the propellors were rotating just above idle speed. These results show that the temperature will fluctuate around 30 degrees, which eliminates any excess heat concern which may affect the UAV.

2.1.1.3. Impact of the distance on surface heating. This experiment shows how effective the lamps are at heating an aerospace-grade composite sample from half a metre and one metre away. The four bulbs were switched on simultaneously for 30 seconds and the temperature of the sample was observed. The experimental setup is shown in Figure 7.
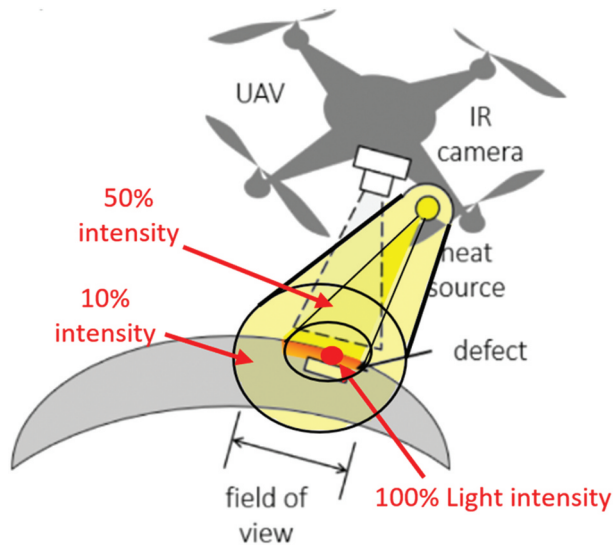
Figure 11. The image shows the beam angle and field angle from a light source onboard a UAV.

The graph in Figure 8 shows the temperature rise of the composite sample whilst being excited by the four 250 W lamps at both half a metre and one metre. A source closer to the samples is of course more effective, at half a metre the temperature increase is approx. 9°C after 30s whilst it reaches only a 2.5°C rise when located at one metre. It would take approx. 8 s to reach a deltaT of 2.5°C at half a metre (vs. 30s at one metre). Hence, a half a metre distance between the source and the sample would be a better choice

The previous experiments have proven that the bulbs can successfully produce enough energy to heat the sample effectively. The propellor wash is beneficial to the lamps as it cools them during the power cycle. However, the propellors may have a direct effect on the heating of the sample of interest.

The following experiment aims to understand the effect of the propellor wash whilst exciting a composite sample. The UAV is connected to a rig and two lamps are placed directly below the propellors. The composite sample is half a metre away from the excitation source. The lamps are switched on and the thermocouple probe is measuring the temperature of the sample. For reference, in Table 4, both Tests 3 and 4 show the increase of the temperature of the sample with two bulbs from half a and one metre distances. Figure 9 shows the experimental setup.

Figure 10 is a graph showing the temperature of the composite sample during excitation (half a metre distance) from the halogen lamps. The temperature of the composite is rising normally until the propellors started rotating at around 25 seconds, which directly affected the heating of the sample. The thrust percentage was slightly over idle. The graph signifies that when the thrust is increased, the temperature of the sample lowers. The fluctuation of temperature on the sample will result in distorted data which will provide inaccurate thermographic results. The graph shows the temperature of the composite sample when subject to the halogen lamp excitation from a one metre
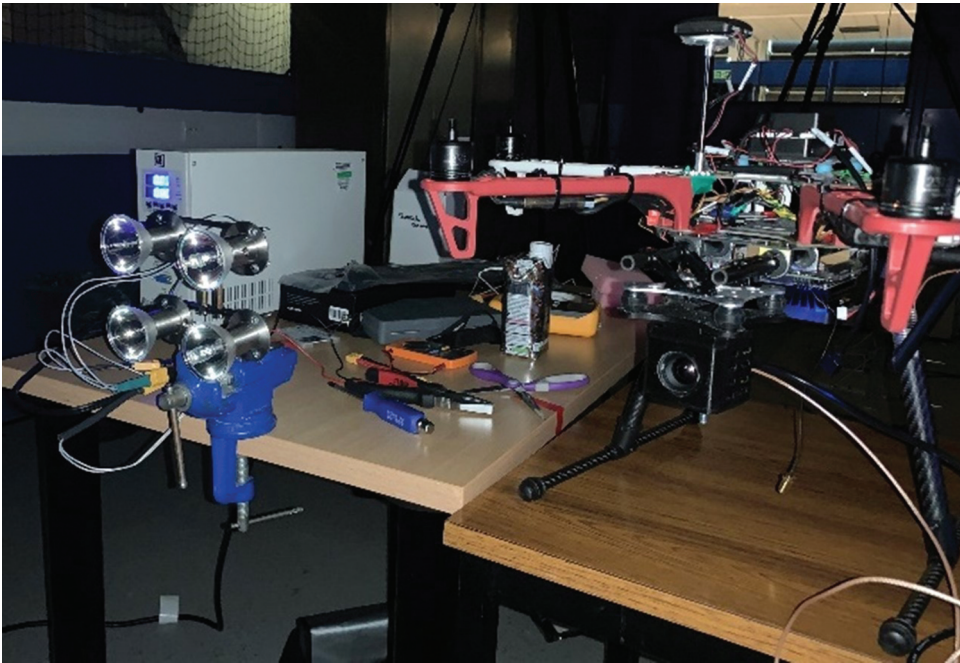
Figure 12. UAV with a thermal camera mounted.

distance. The temperature is rising normally, and the propellors start rotating at 25 seconds. The graph shows that the propellor wash does not affect the temperature of the sample like it did when the UAV was half a metre away from the sample.

To summarise, the results in the experiments in section 2.1.1 show that the chosen lamps are effective at heating the composite sample from multiple distances whilst the subsequent lamp temperature does not affect the serviceability of the UAV itself. The purpose of the multiple distance experiments was to understand the optimal flight distance from the subject of interest during an inspection. From these experiments, it can be concluded that half a metre between the source and the inspected surface is adequate for heating the sample, but the data also shows that it is not a feasible distance for an inspection due to the interference of the sample excitation from the UAV propellors. Therefore, one metre would be the ideal inspection distance.

2.1.1.4. Beam angle. The beam angle is the angle at which the lamps distribute and emit light. The beam angle will help understand the amount of energy that hits the surface in a specific area. This is important as uniform heating is required for active thermography, so the dataset is accurate. The absence of a lens and/or reflector means that the emitted light beam will distribute the energy within a wide area. The halogen lamps will emit energy given in degrees, subsequently, a 'light circle' will be produced. This light circle can be seen in Figure 11.
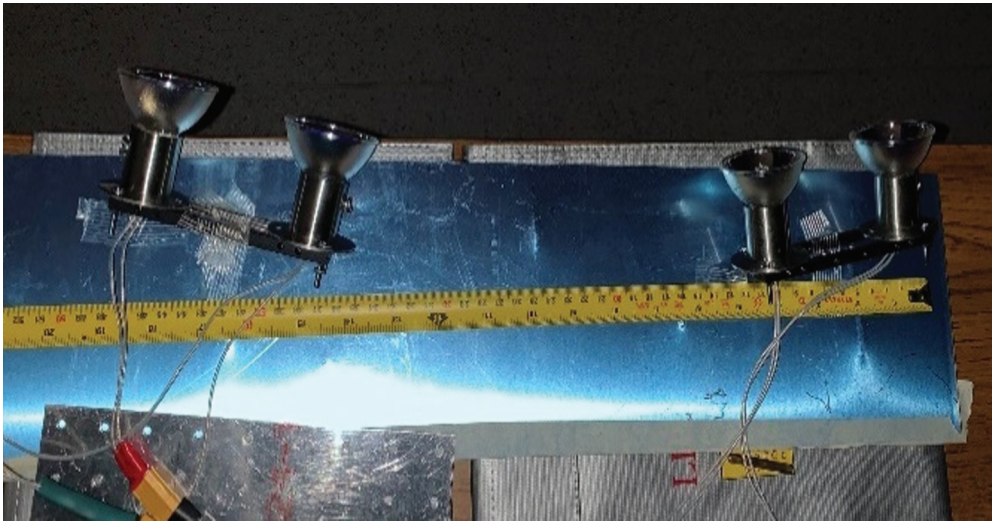
Figure 13. Two lamps 20 cm apart from the other two lamps.

The beam angle is defined as a minimum of 50% or more of its maximum luminous intensity. Directly in the centre is the only place where the luminous intensity would be maximum (100%). Intensity is equal to the energy per second on a 1 m^2 area. Further to the beam angle, the field angle can be seen light circle where one-tenth (10%) of the lamp is radiated [8].
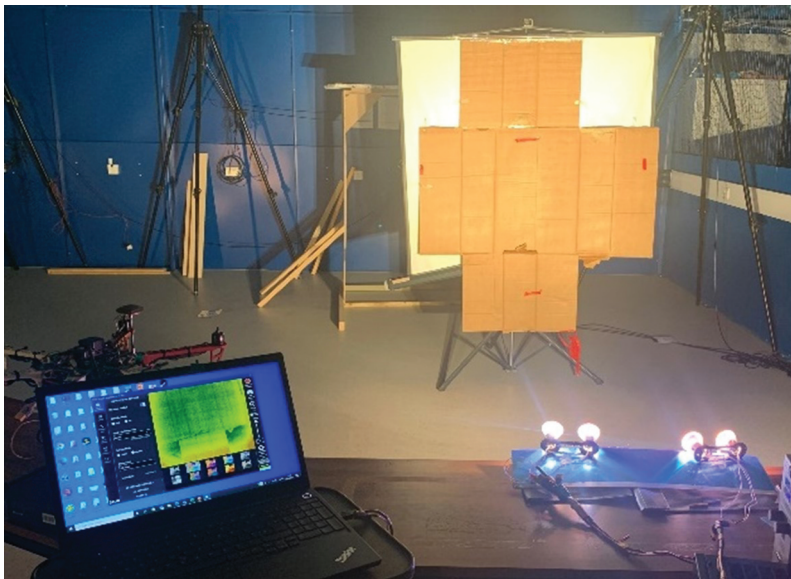

Figure 14. Experimental setup and the lamps exciting the surface. The laptop is connected to the thermal camera for analysis of the excitation. The UAV is fixed during the experimentation.
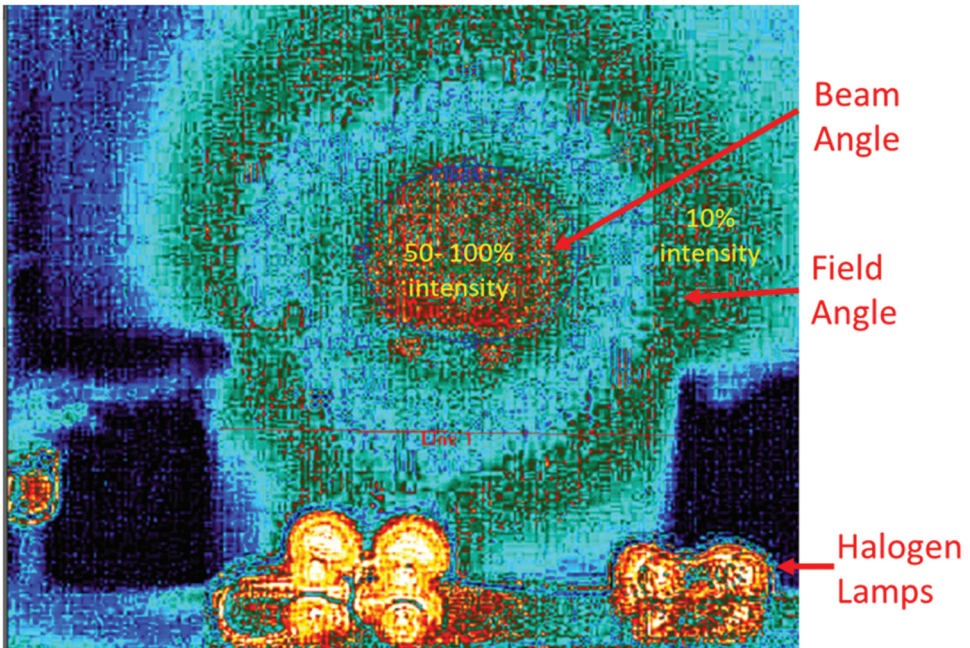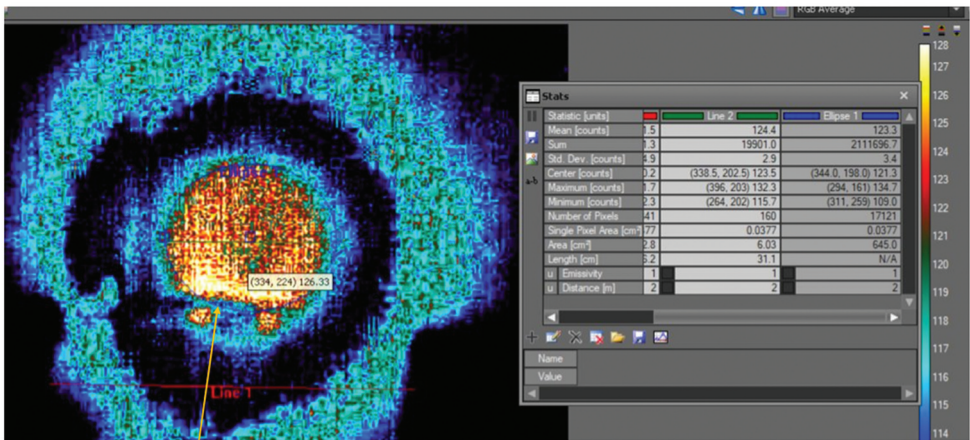
Figure 15. An infrared image of the halogen lamps exciting a surface.

Using Equation 2, the direct relationship between the beam angle, the diameter of the light circle and the distance to the illuminated sample can be calculated. The optimum beam angle for the UAV inspection can be calculated. Where **a** is the Beam angle in

Diameter: 31.1cm (0.9284777ft)
Distance: 100cm (3.28084ft)
Beam Angle: 17.7° (100-80 intensity)

Four Bulbs parallel at 1 metre away
Camera 640x512: HFOV 24deg

Figure 16. The image is a screenshot from the ResearchIR software showing an IR image taken of the bulbs exciting a surface. A line is drawn across the uniform excited surface and the details can be seen in the table within the image named 'Line 2'.
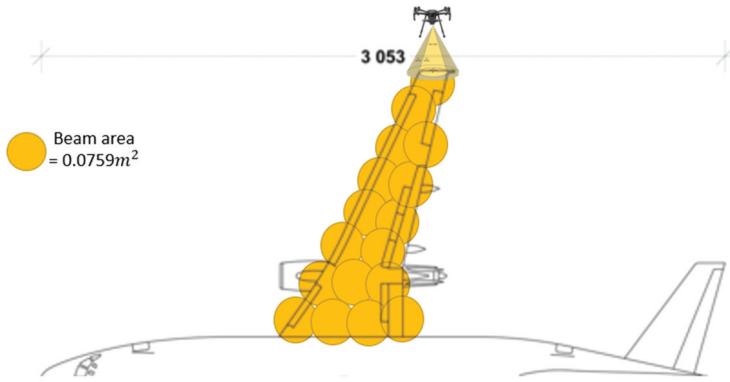
Figure 17. Static active thermographic inspection onboard a hovering UAV. The yellow circles represent the beam area.

degrees, **Ø** is the diameter of the illuminated area of interest in feet, **D** is the distance between the lamp and area of interest in feet and **Arctan** is the inverse function of the tangent for angle calculation.

Equation 2: Beam Angle Formula [9].

$$a = 2 \cdot (\mathbf{Arctan}(\frac{\emptyset}{2 \cdot d})) \tag{2}$$

Table 5. Active thermography experimental configurations.

Number of bulbs.	Time.	Distances.
2 bulbs.	1s, 2s, 5s, 10s, 15s.	Half a metre, one metre.
4 bulbs.	1s, 2s, 5s, 10s, 15s.	Half a metre, one metre.

Figure 18. (A) An image of the active thermography experimental setup with two halogen lamps. **(B)** An image of the active thermography experimental setup with four halogen lamps.

Table 6. The table shows the optimal excitation time in seconds for both two and four bulb setups.

Number of bulbs	Optimal heating time
2 bulbs	5 s
4 bulbs	2 s

The following test will aim to calculate the beam angle of four 250 W halogen lamps. The four bulbs are angled inwards with two bulbs on each side at 20 cm apart to replica a UAV mounting position. A thermal camera is used to measure the diameter of the beam angle (the 50% or more luminous intense area). Figure 12 is an image of the UAV with a thermal camera mounted and the four halogen lamps.

The lamps were switched on simultaneously at half a metre from the surface. The thermal camera is analysing the surface throughout and capturing the IR waves. Figures 13 & 14 show the experimental setup.

ResearchIR is a thermographic image processing tool that can locate a uniform intensity region from the data captured. This tool is used to analyse the captured thermographic data using spatial calibration, the beam and field angles can be determined by knowing the FOV of the camera. To spatially calibrate the thermal image, one of the four methods below can be used.

(1) Calculate from camera FOV (FPA width, FPA height & FOV degrees).
(2) Calculate from focal length (pixel pitch, Focal length).
(3) Measure a known object length and distance from the object.
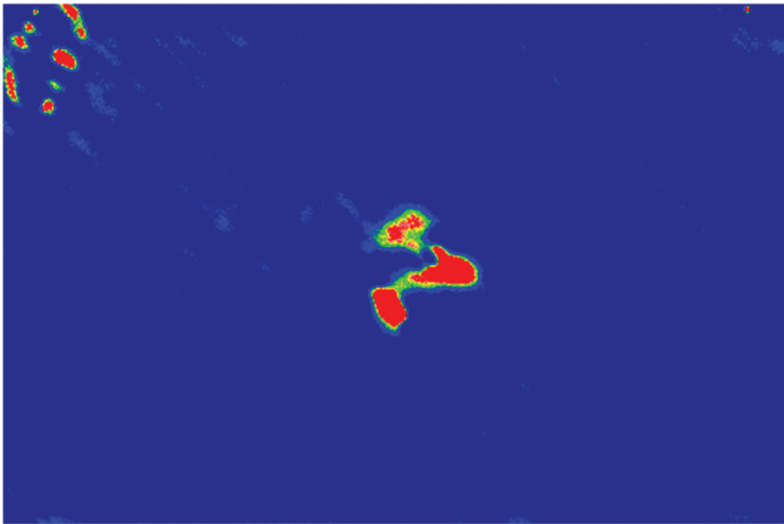(4) Enter manually the instantaneous vertical field of view (IVFOV) and instantaneous horizontal field of view (IHFOV)

Figure 19. Thermogram showing the result of the active thermographic inspection of an impacted composite sample 24 J of impact damage. The camera was captured data at 25 Hz.
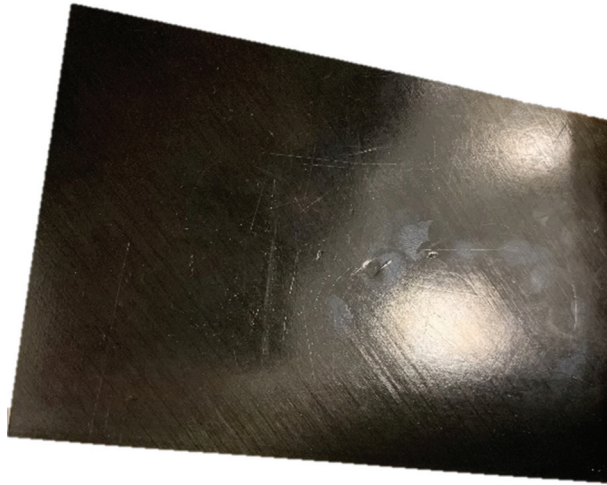
Figure 20. Visible image of the sample tested in Figure 19.

Once the images are spatially calibrated, the diameter of the focused area can be measured by drawing a line within ResearchIR across the uniform heated circle. The diameter and the distance between the camera and the surface can be inputted into Equation 2 which will output the beam angle. Figure 15 is an infrared image of the lamps exciting a surface. The beam angle and field angle can be seen with regard to the false colour differences in the image. The colour differences represent the intensity of the infrared energy distribution across the surface.

Figure 16 shows the thermal image of the emitted radiation from the four lamps. The diameter of the uniform circle within the beam angle is **31.1 cm** and the distance is **one metre** which was previously decided in the previous experiments. The calculated beam angle is **17.7 degrees**. This region shows the area that can be inspected when the UAV is static during the flight. The diameter (31.1 cm) can be divided by the specimen size which will give the number of inspections needed during the flight.

The radius of the uniform beam is 15.55 cm, as it is the diameter (31.1 cm) divided by 2. The area of the beam can be calculated by multiplying π by the radius squared as seen in Equation 3. The area of the uniform excitation beam is 0.0**75964496 m^2.**

Equation 3: Area of a circle.

$$\pi x 15.55^2 = 759.64496\textbf{cm}^2$$
$$A = \pi r^2 \quad 759.64496\textbf{cm}^2 = 0.075964496\textbf{m}^2$$

(3)

It is now possible to calculate how many acquisitions will take place during an inspection of a specimen. To do this, the area of interest is divided by the using the area of the excitation beam as seen in Equation 4.

Equation 4

$$I = \frac{SOI}{EAB}$$

(4)

Figure 21. (A) An image of the FLIR Boson and the Zenmuse XT. **(B)** An image of the composite sample.

Where:

    SOI = *Specimen of interest in* $\mathbf{m}^2$

    EAB = *Excitation area beam in* $\mathbf{m}^2$

    I = *Number of acquisitions*

For example, when inspecting a Boeing 737 wing which has an area of **125 m²** it would take 1645 inspections to capture a dataset of the whole wing as seen in the following calculation.

$$\frac{125\mathbf{m}^2}{0.075964496\mathbf{m}^2} = 1645 \; \textbf{acquisitions}$$

Figure 17 is an example of the static active thermographic inspection onboard a hovering UAV.

It is important to keep a constant inspection distance for reliable results. When the distance is increased, the inverse square law means the luminous will distribute to a larger area, subsequent of this, the FOV of the lamps would increase but the amount of excitation will be reduced resulting in the sample not being heated effectively.

3. Experimental procedure II

3.1. Optimal excitation for composite pulsed thermography

The following experimental procedure aimed to understand how effective multiple 250 W small halogen lamps are when used for long pulse active thermography. Usually, larger and more powerful lamps (in terms of wattage) are used for active thermography. The experiments used the lamps for inspecting a composite sample. This helped to determine whether the lamps can provide sufficient infrared energy to propagate through the composite material promptly.

3.1.1. Optimal excitation using a high-end cooled camera

Testing at Université Laval (Canada) assisted in understanding the required heating time parameters for a pulsed thermographic inspection of composites using four 250 W halogen lamps. The lamps were used to inspect a composite sample and the data was captured using a high-end cooled camera (FLIR X8502sc, MWIR, InSb, 3–5μ, 1280 × 1024 pixels).
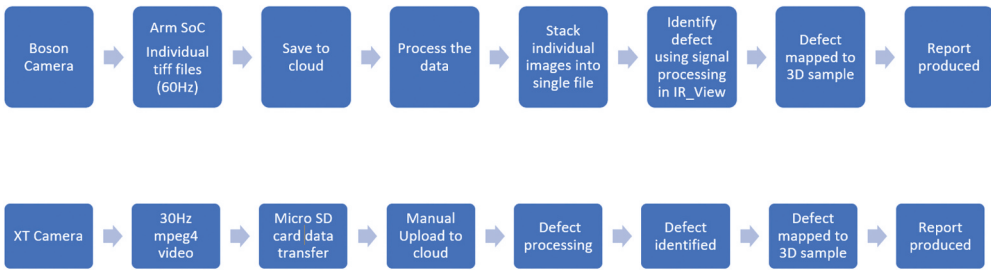
Figure 22. Thermal data acquisition and processing flow for the UAV system.

The composite samples are subject to heating with regards to the configurations in Table 5. The experimental setup can be seen in the images in Figure 18.

The images captured from the camera were analysed using multiple active thermography post-processing techniques. For the two-bulb configuration, the data was processed for each heating time. The optimal defect detection time was observed when the sample for a total of 5 s, regardless of the distance (half a metre or one metre). For the four-bulb setup, the optimal heating time was reduced to 2 s for both half a metre and one metre. Due to the sensitivity of the camera, the results show that the longer the heating time, the more thermally saturated the sample became, which subsequently distorted the data. Table 6 shows the results of the experiments.

The results show that composites can be inspected using two or four 250 w halogen bulbs for excitation. Establishing the optimal heating time is critical since it provides guidance about the minimum required energy to inspect a composite section, which is of paramount importance for a UAV inspection. However, the results are only representative of a high-end cooled system, which is not feasible to mount onto a UAV due to the weight of the camera and the power required to operate it. Nevertheless, these results provide a good indication about the expected heating time when using an uncooled thermal camera on a UAV.

3.1.2. Optimal excitation using a low-power uncooled camera

Before mounting a thermal camera onto the UAV, the competency of the camera needs to be thoroughly tested to observe its capabilities. Therefore, a low-power/small/low-weight uncooled IR camera (FLIR Boson, LWIR, 640 × 512 pixels), which is the proposed camera for the UAV, is used in the following experiments for the NDT of aerospace composite structures. The following experiment aimed to provide the optimal excitation time with four halogen lamps for pulsed thermography, using such camera.

A composite sample was inspected to understand the effectiveness of locating subsurface damage using different long pulse durations. Figure 19 is a post-processed image showing the true extent of the damage. The sample (Figure 20) has a known impact (24 J) defect and has been inspected using a TWI (Thermal wave imaging) system to see the extent of the damage. Figure 20 is an image of the sample showing the extent of the damage to the naked eye.

Figure 21A is an image of the UAV with two cameras mounted, Zenmuse XT and FLIR Boson. The two microbolometer cameras are used to capture active thermographic data. Figure 21B shows the composite sample (same sample as in Figure 19) that has a known defect (24 J impact damage).
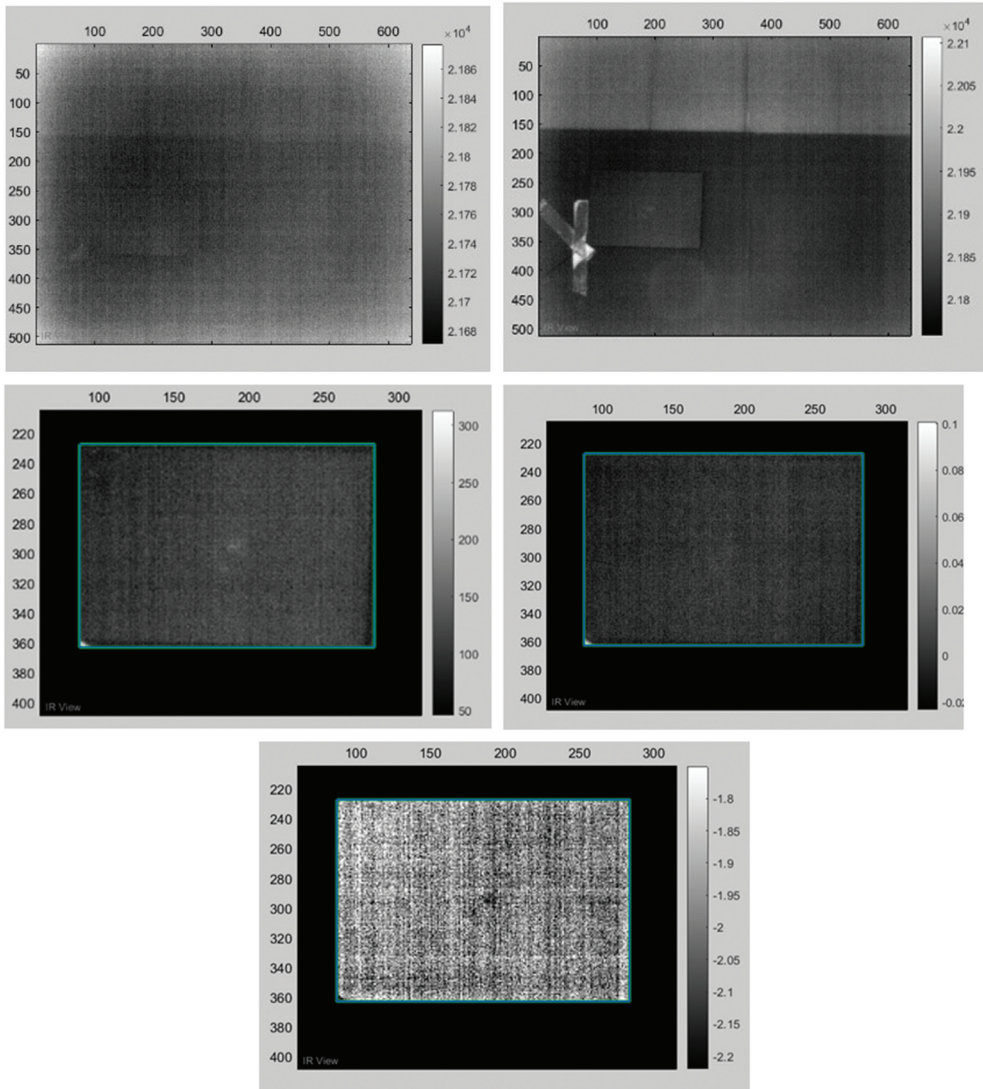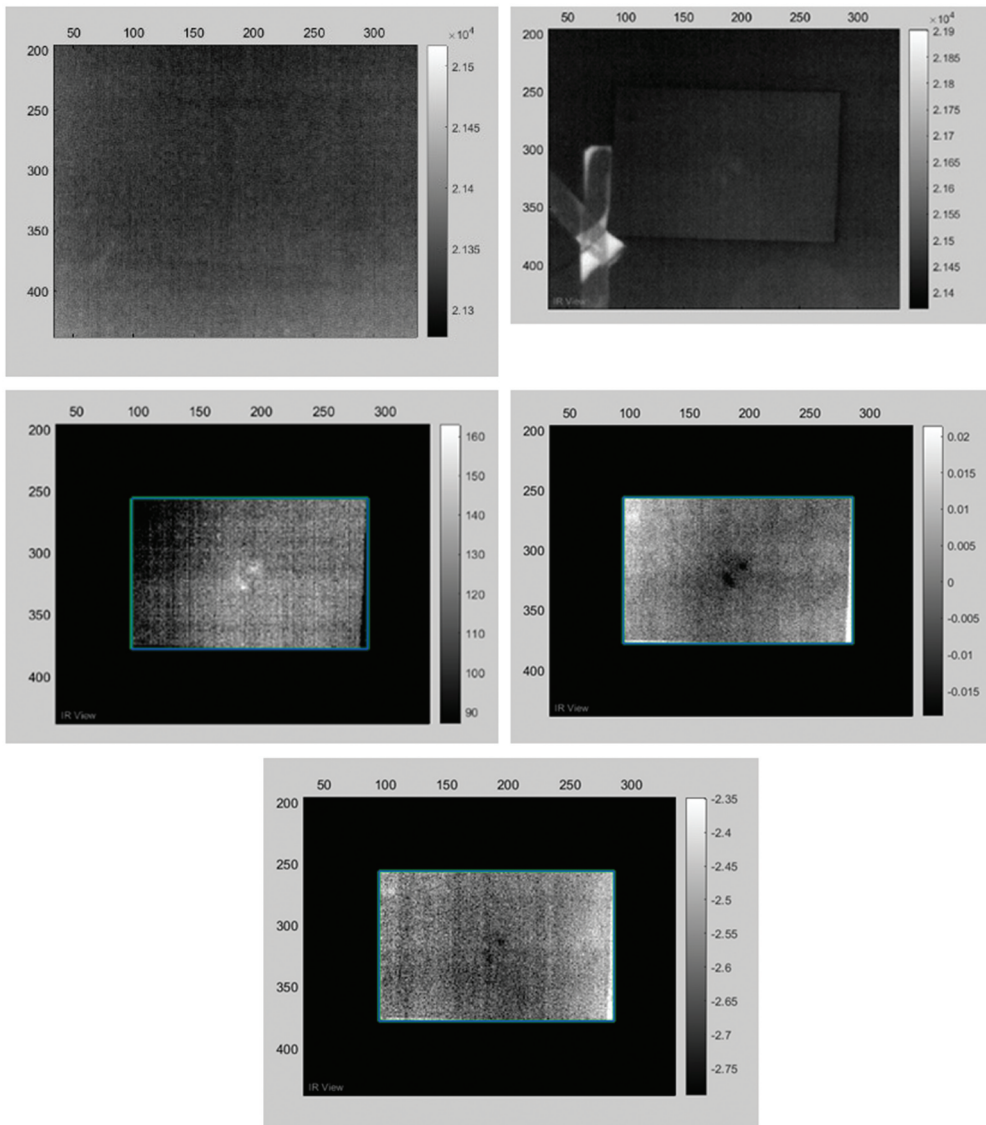
Figure 23. (A) A raw thermal image (**Frame 1 cold image**). **(B)** A raw image immediately after thermal excitation (**Frame 59**). **(C)** The thermal image after cold image subtraction (**Frame 58**). **(D)** The thermal image after PCT has been performed (**EOF 7. PCT 1.8%**). **(E)** The thermal image after PPT has been performed (**f = 60 Hz**).

Table 7. The table shows the calculated values from all tests.

Excitation time (plus 60s post-heating capture time)	Total number of frames (TNF)	Frames per second (FPS)	Total inspection time (TT)
2 s	291 Frames	4.17 fps	46.28 s
5 s	294 Frames	3.93 fps	41.98 s
10 s	240 Frames	2.61 fps	45.5 s
15 s	235 Frames	3.13 fps	41 s

Figure 24. (A) A raw thermal image (**Frame 1 cold image**). **(B)** A raw image immediately after thermal excitation (**Frame 67**). **(C)** The thermal image after cold image subtraction (**Frame 65**). **(D)** The thermal image after PCT has been performed (**EOF 3. PCT 2.9%**). **(E)** The thermal image after PPT has been performed (**f = 60 Hz**).

It is worth mentioning that the two different cameras acquire data differently. The FLIR Zenmuse XT captures in mpeg4 at 30 Hz and will save it to the local SD card, whereas the FLIR Boson can capture a sequence of tiff images at 60 Hz and can store the captured data to the cloud. This means that the data processing methods are different for each camera. Figure 22 is a flow chart detailing the methods from acquiring the thermal data to the final inspection report.
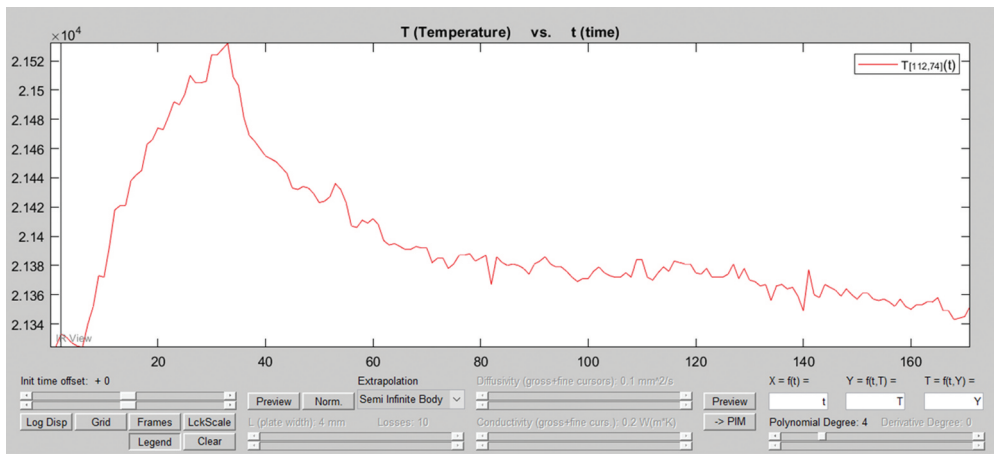
Figure 25. Temperature over time graph from a pixel within the sample on the thermogram.

In the following experiments, active thermography was used to inspect the composite sample. The excitation consisted of four 250 W halogen lamps with excitation durations of 2, 5, 10 and 15s. The lamps were mounted on carbon fibre poles allowing them to be extended from the centre of the UAV and be closer to the sample. The camera is at a 1.2 m distance from the sample and the four lamps are 0.75 m away. The following processing techniques are used:

- **Pulsed phase thermography (PPT)** transforms the data from the time domain into the frequency domain using one-dimensional discrete Fourier transform [10].
- **Principal Component Technique (PCT)** is a technique used to identify patterns in data, such as the similarities and differences, whilst also compressing the data without losing much information [10].
- **Cold image subtraction** is a signal processing technique that removes fixed patterns such as noise and fixed environmental reflections. The cold image is usually a thermogram acquired before any thermal excitation [10].

3.1.1.1. Two seconds excitation (test A). The lamps excited the sample for two seconds whilst the IR camera observed throughout and for a further 60 seconds post-excitation (cooling phase). Figure 23 shows five IR images at different stages of processing. Figure 23A has not been modified and is the cold image from the IR camera. Figure 23B is a frame just after the thermal excitation. Figure 23C is the image after the cold image has been subtracted. Figure 23D is an image after PCT post-processing and Figure 23E is after phase processing.

The excitation provided a minor contrast difference between the defected and sound area of the sample. There is minimal temperature differentiation as the temperature of the sample has barely increased due to the short excitation. The total inspection time for defect detection for 2 s of heating was 46.28s. The parameters for Test A, B, C and D are shown in Table 7.
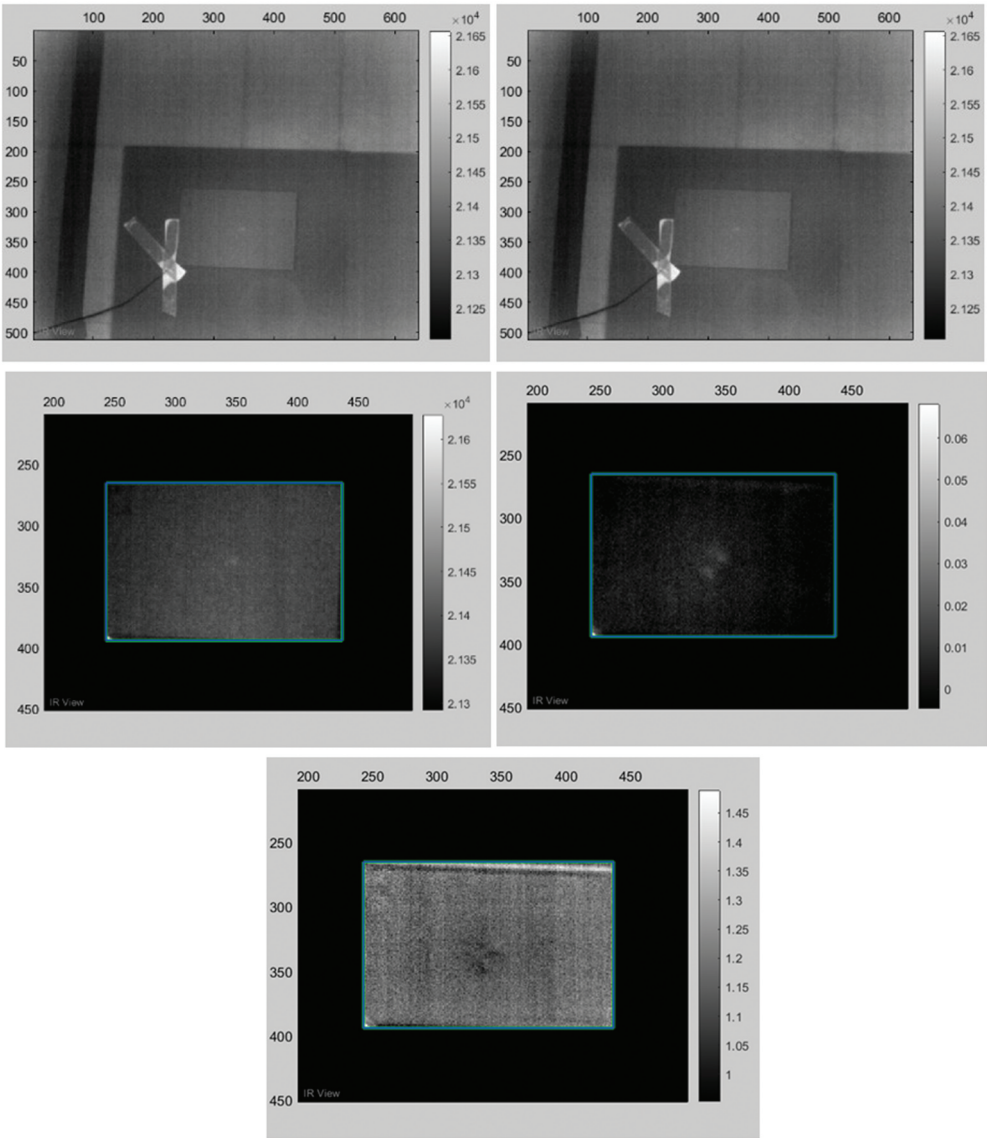
Figure 26. (A) A raw thermal image (**Frame 1 cold image**). **(B)** A raw image immediately after thermal excitation (**Frame 67**). **(C)** The thermal image after cold image subtractions (**Frame 67**). **(D)** The thermal image after PCT has been performed (**EOF 3. PCT 4.8%**). **(E)** The thermal image after PPT has been performed (**f = 60 Hz**).

3.1.1.2. Five seconds excitation (test B). The test was repeated for a 5 s heating. The post-processed images (Figure 24) show a sharper and clearer image of the defect than previously seen with the 2 s of excitation exposure.

The temperature over time graph in Figure 25, shows the composite heating up and then cooling at a slower rate.
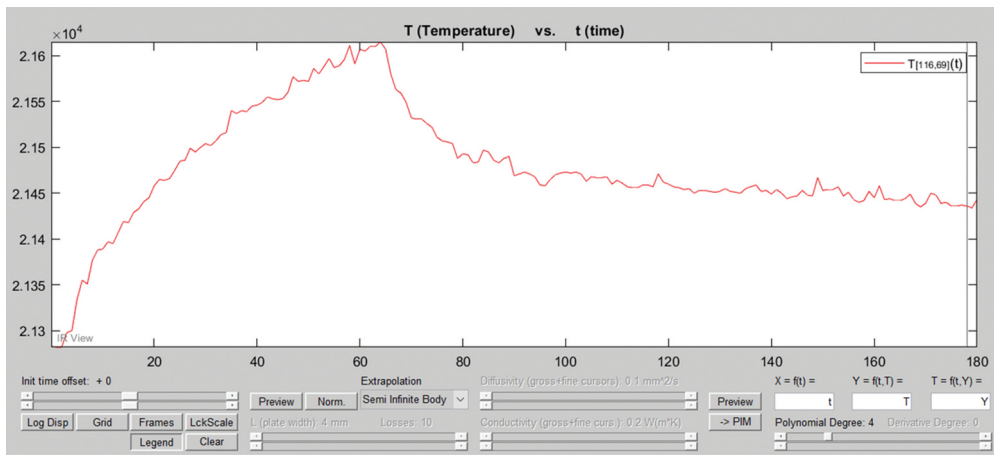
Figure 27. The temperature over time graph from a pixel within the sample on the thermogram.

The optimal total inspection time for **Test B**, is 41.98 seconds with 5 seconds of excitation and 36 seconds of recording the cooling phase.

3.1.1.3. *Ten seconds excitation (test C).* The test was repeated for a 10s heating. Figure 26 shows the results from the IR post-processing of the data.

Figure 27 shows the temperature over time graph for the inspection with a duration of 10 seconds of thermal excitation. The graph demonstrates familiar heating and cooling phases as the lamps have heated the sample effectively during the 10 second period.

The optimal total inspection time for **Test C**, is 45.5 seconds with 10 seconds of excitation and 30 seconds of recording the cooling phase.

3.1.1.4. *Fifteen seconds excitation (test D).* The test was repeated for a 15s heating. Figure 28 shows the results from the IR post-processing of the data.

Figure 29 shows the temperature over time graph for the inspection with a duration of 15 seconds of thermal excitation.

The optimal total inspection time for **Test D**, is 41 seconds with 15 seconds of excitation and 26 seconds of recording the cooling phase.

3.1.3. *Results and discussion*

To conclude, regardless of the excitation time, the results show that an average of 43.69 seconds of inspecting one area is optimum. An excitation for a duration of between 5–10 seconds will likely be the ideal excitation time to comply with the onboard power requirements. Table 7 shows the values from all four inspections with the different excitation times.

In section 2.1.1.4. an estimated 1654 inspection datasets would complete a full wing area inspection of a Boeing 737. Therefore 1654 multiplied by 43.69 seconds would give a total of 20 hours inspection time of one wing. A further reduced capture time is possible, however, it is possible that the quality of the data would be affected and the likeliness of locating the subsurface defects would be reduced. The data after excitation is essential as
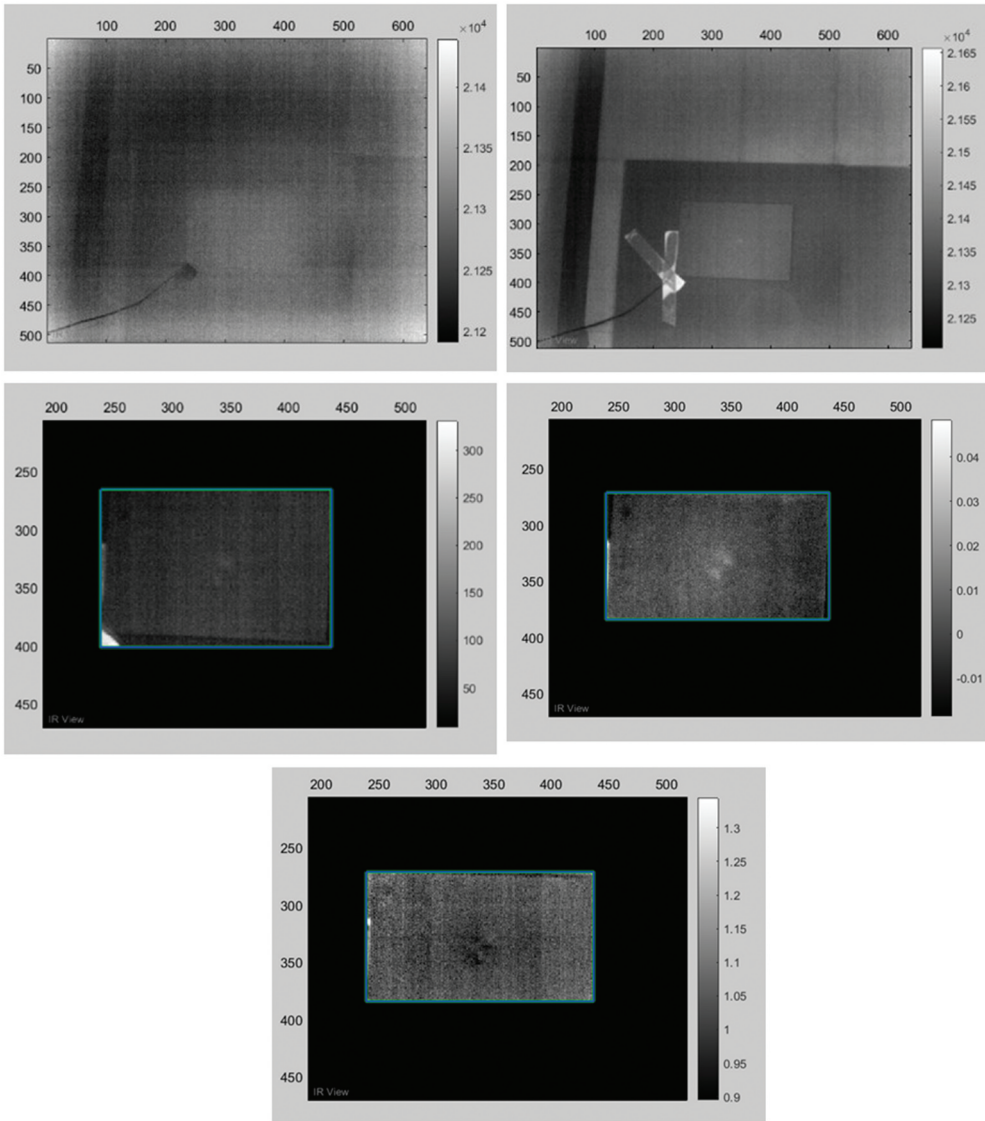
Figure 28. (A) A raw thermal image (**Frame 1 cold image**). **(B)** A raw image immediately after thermal excitation (**Frame 67**). **(C)** The thermal image after cold image subtraction (**Frame 65**). **(D)** The thermal image after PCT has been performed (**EOF 3, PCT 4.5%**). **(E)** The thermal image after PPT has been performed (**f = 60 Hz**).

the temperature decay curve is important for the post-processing phase. Further experimentation will aim to reduce acquisition time to around 20 seconds and reducing the frame rate to 30 Hz may reduce noise.

Figure 30 is a series of PCT images after reconstructing the thermal signal with a derivative degree of 7. Thermal signal reconstruction has improved the detectability of the defect and provided sharper images all around.
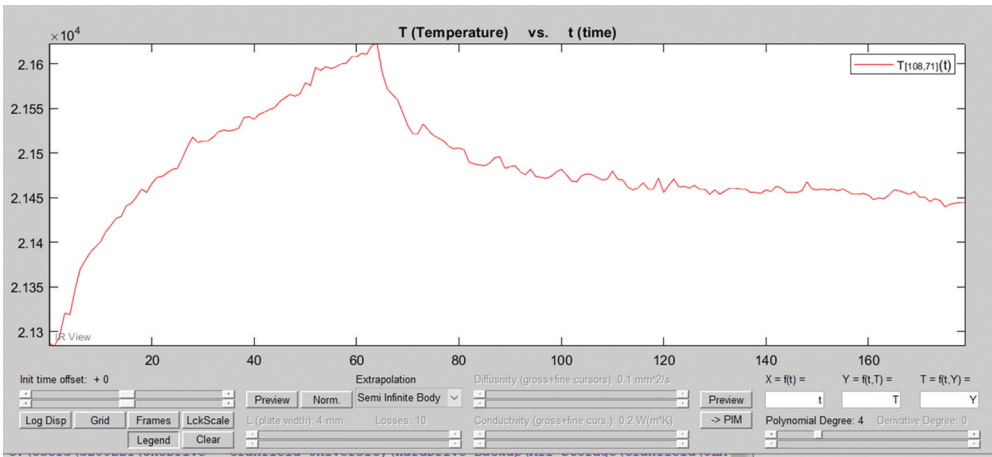
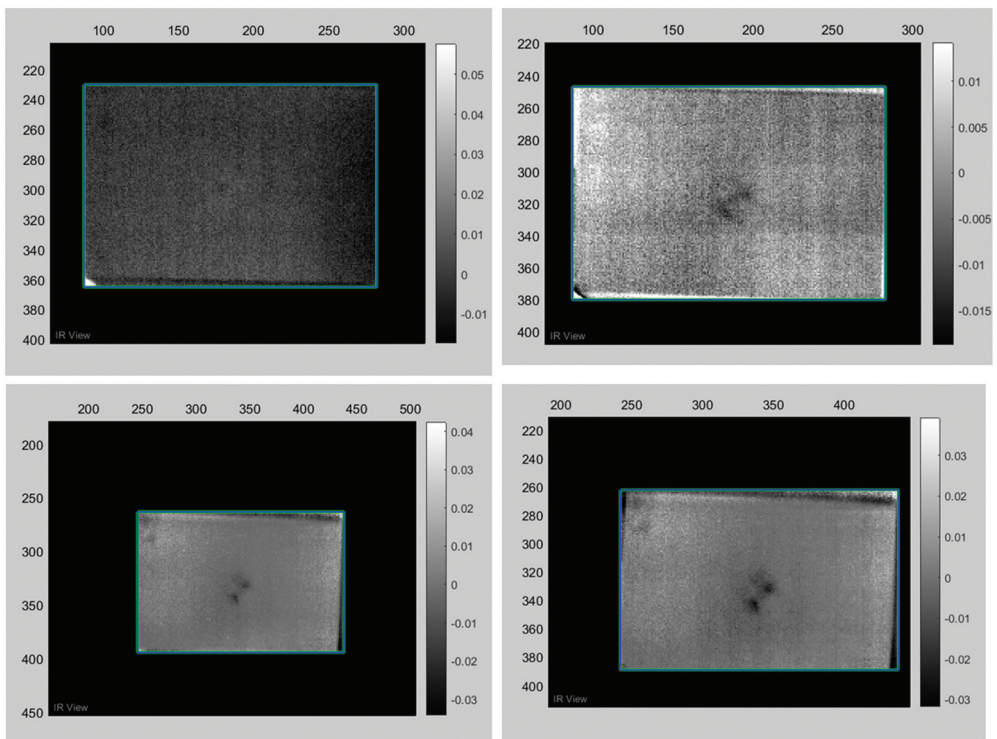**Figure 29.** The temperature over time graph from a pixel within the sample on the thermogram.

Figure 30. (A) The thermal image after PCT has been performed from the dataset with 2 seconds of excitation (**EOF 9**). **(B)** The thermal image after PCT has been performed from the dataset with 5 seconds of excitation (**EOF 9**). **(C)** The thermal image after PCT has been performed from the dataset with 10 seconds of excitation (**EOF 9**). **(D)** The thermal image after PCT has been performed from the dataset with 15 seconds of excitation (**EOF 9**).
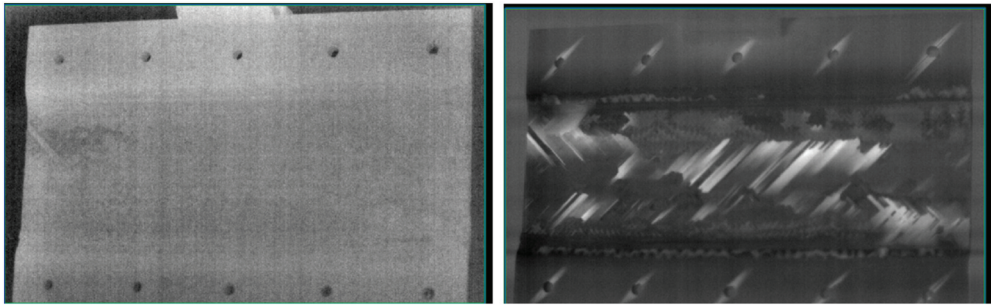
Figure 31. (A) A cold image of a damaged composite sample before excitation. **(B)** A thermal image of a post-processed image of a composite sample after excitation.

From the series of inspections with excitation times 2, 5, 10 and 15 seconds, in this instance, the defect visibility increased with the longer time duration of excitation. This is not always the case, as sometimes the excess heat can saturate the data. The UAV inspection requires the shortest excitation time due to the power limitations, therefore 2 seconds excitation would be the preferred option, however, the defect is not visible in the output data. The preferred excitation from the lamps onboard the UAV is a minimum of 5 seconds. The image is not sharp at 5 seconds, but it is sufficient as the defect is visible. The more capacity of the battery that the UAV can carry, the longer the excitation time could be. Alternatively, a tethered solution would enable a full 15 seconds of excitation or more if needed.
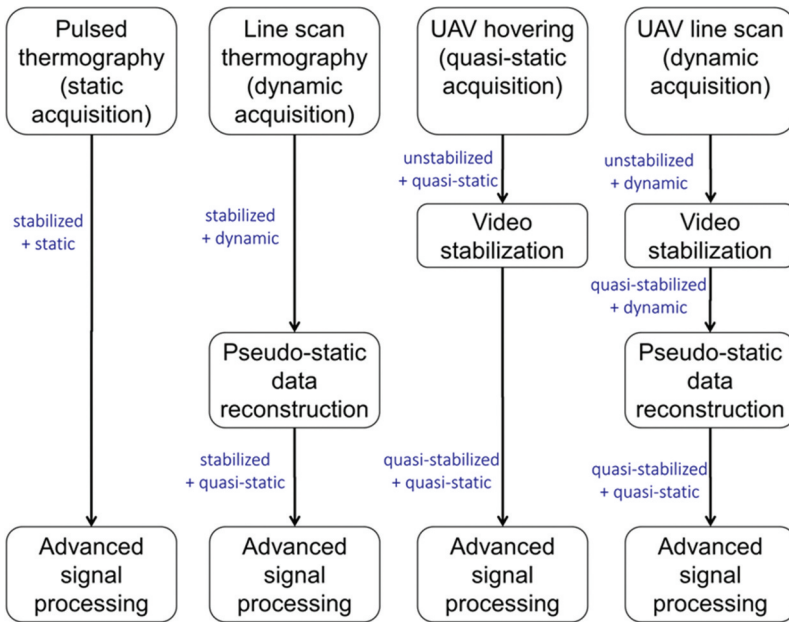

Figure 32. Dynamic and static thermography approaches.

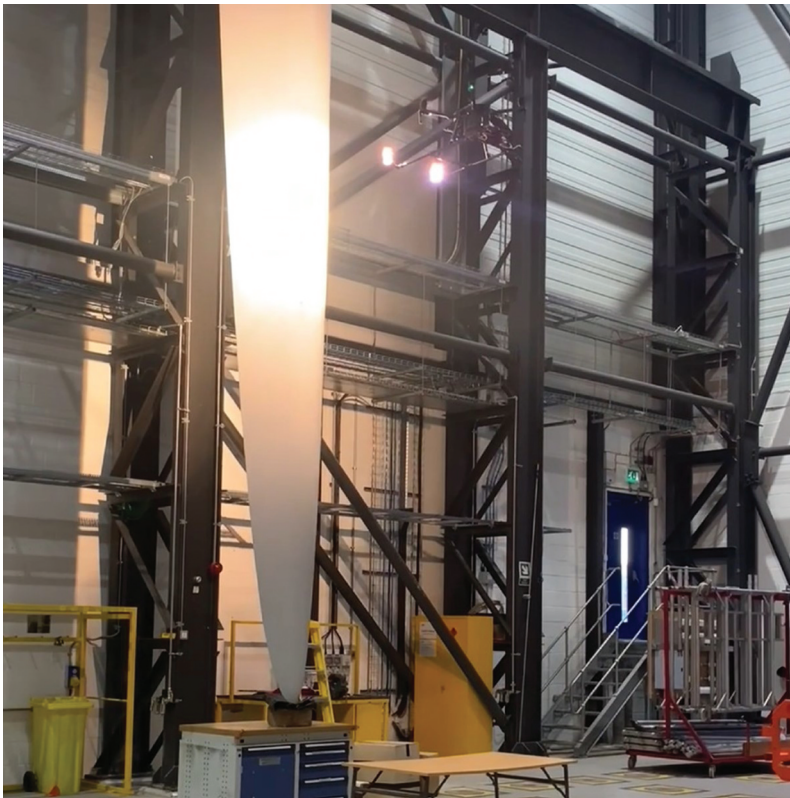**Figure 33.** Developed focus mechanism for the FLIR Boson.

Figure 34. The active IR drone platform inspecting a composite wind turbine blade.

Figure 31A is a raw (unprocessed) cold image, as expected, passive thermography does not show any defects. Whereas Figure 31B shows a post-processed image after thermal stimulation. The processed image displays the torque damage from screw holes, such damages can be common with composites if the correct procedures are not followed accurately. The sample has delamination and fibre breakage.

The diagram in Figure 32 illustrates the steps needed to process data from an active thermographic UAV. The approach which has been taken in this research is the 'UAV hovering'. In Figure 32, the diagram shows the increase on complexity starting with the classic PT approach to a dynamic UAV scanning. UAV line scan is the most complex acquisition method it may however greatly increase the speed of active thermographic inspections.

4. Conclusion

The research performed and presented in this paper, delivered a successful active thermographic excitation source that is suitable for a UAV platform. Multiple scientific experiments proved that the lamps chosen could provide enough energy to excite a composite structure effectively for the localisation of damages using thermography and further signal processing techniques.

Further experiments proved that the lamps could be mounted on the UAV without interference from the propellors and the lamps could be powered entirely with an onboard battery. This allows the UAV to be completely versatile and not rely on a tethered power supply. The inspection area of the active thermography UAV from 1 metre away, was calculated at approximately 760 cm2 (118 in2) in 43s. Going forward, these values can help calculate the inspection time of a structure with known dimensions.

It is essential that the UAV maintains a predefined distance from the area of interest to ensure the consistency of the thermal lens with respect to the region of interest. To maintain the distance, motion capture systems track the UAV in 3D space and time and feed localisation data back to the UAV system to guarantee millimetre accuracy. Other systems are in place, such as range finder LIDARs to measure the distance to the area of interest. A mechanism has been developed to remotely adjust the FLIR Boson camera focus. This is a failsafe option in case the localisation system fails, and the distance has changed between the camera and the area of interest, this would result in an out of focus image and corrupt the captured data. See Figure 33 for the camera mechanism and the feedback via WIFI to the ground station. A developed GUI controls the focus.

For the aircraft inspection, to ensure the lamps are half a metre or one metre away, the lamps are extended from the UAV body as seen in Figure 1. The motion capture localisation system and onboard collision avoidance sensors ensure it is safe to inspect the aircraft at such a close distance. It is possible that half a metre would have come with a risk, due to the turbulent draft from the UAV, which was considered, however the outcome of the thermography results prove that the one metre distance is sufficient for inspection. Figure 34 is an image of the active IR system inspecting a composite wind turbine blade from one metre away. This demonstrates the possibility to safely conduct inspections using this platform and the versatility of inspecting different area of interests.

Finally, this work demonstrated effective signal processing techniques that can assist in identifying subsurface damages on composites from multiple distances.

Acknowledgments

Disclosure statement

No potential conflict of interest was reported by the author(s).

Funding

ORCID

Shakeb Deane 🄳 http://orcid.org/0000-0002-6414-1166
Xavier P. V. Maldague 🄳 http://orcid.org/0000-0002-8777-2008

Nomenclature

Ø	Diameter of the object or surface to be illuminated
π	Pi
a	Beam angle
A	Area of circle
Arctan	Inverse function of the tangent for angle calculation
AWG	American wire gauge
D	Distance between lamp and object or surface
EAB	Excitation area beam in M^2
FoV	Field of view
FPA	Focal Plane Array
FPS	Frames per second
IFOV	Instantaneous field of view
IHFOV	Instantaneous horizontal field of view
IVFOV	Instantaneous vertical field of view
IRT	Infrared thermography
I	Number of acquisitions
LST	Line scan thermography
NDT	Non-destructive testing
PT	Pulsed thermography
PPT	Pulse phase thermography
R	Radius
RGB	Red, green, blue
SOI	Specimen of interest in m^2
TNF	Total number of frames
TSR	Thermographic signal reconstruction
TT	Total inspection time
TWI	Thermal wave imaging
UAV	Unmanned aerial vehicle

References

[1] Avdelidis NP, Almond DP, Dobbinson A, et al. Aircraft composites assessment by means of transient thermal NDT. Prog Aerosp Sci. 2004;40(3):143–162.

[2] Ibarra-Castanedo C, Sfarra S, Klein M, et al. Solar loading thermography: time-lapsed thermographic survey and advanced thermographic signal processing for the inspection of civil engineering and cultural heritage structures. Infrared Phys Technol. 2017;82(May):56–74.

[3] Ibarra-Castanedo C, Brault L, Genest M, et al. 2012. Detection and characterization of water ingress in honeycomb structures by passive and active infrared thermography using a high-resolution camera. Proc. QIRT 11 – Quantitative Infrared Thermography, paper number: QIRT-2012-278, Naples, Italy.

[4] Kidangan RT, Krishnamurthy CV, Balasubramaniam K, (New 4) Renil Thomas Kidangan, Chitti Venkata Krishnamurthy & Krishnan Balasubramaniam. Detection of dis-bond between honeycomb and composite facesheet of an Inner Fixed Structure bond panel of a jet engine nacelle using infrared thermographic techniques. Quant Infrared Thermogr J. 2022;19(1):12–26.

[5] Zhang H, Avdelidis NP, Osman A, et al. Enhanced infrared image processing for impacted carbon/glass fiber-reinforced composite evaluation. Sensors. 2017;18(2):45.

[6] Nave Carl Rod Department of Physics and Astronomy, Georgia State University 2017. Inverse square law. Hyperphysics.Phy-Astr.Gsu.Edu [cited 2021 Dec 10 2021]. Available from http://hyperphysics.phy-astr.gsu.edu/hbase/Forces/isq.html.

[7] Martin B 2017. Choose the right gauge wire size for your application. Blog.Powerandtest.Com [cited 2021 Dec 10]. Available from http://blog.powerandtest.com/blog/choose-the-right-gauge-wire.

[8] Amazon Services LLC Associates Program. 2021. *Beam Angle And Field Angle*. Image [cited 2021 Dec 10]. Available from https://lamphq.com/beam-angle/.

[9] «LED beam angle guide » beam angle calculator - Lamphq". 2021. *Lamphq* [cited 2021 Dec 10]. Available from https://lamphq.com/beam-angle/#beam-angle-calculator.

[10] Deane S, Avdelidis NP, Ibarra-Castanedo C, et al. Comparison of cooled and uncooled ir sensors by means of signal-to-noise ratio for NDT diagnostics of aerospace grade composites. Sensors. 2020;20(12):3381.